A plume model of transient diachronous uplift at the Earth's surface

John F. Rudge [a,b,*], Max E. Shaw Champion [a], Nicky White [a], Dan McKenzie [a], Bryan Lovell [a]

[a] *Bullard Laboratories, Department of Earth Sciences, Madingley Rise, Madingley Road, Cambridge CB3 0EZ, UK*
[b] *Institute of Theoretical Geophysics, Department of Applied Mathematics and Theoretical Physics, Centre for Mathematical Sciences, Wilberforce Road, Cambridge CB3 0WA, UK*

Abstract

Convection in the Earth's mantle appears to be strongly time-dependent on geological time scales. However, we lack direct observations which would help constrain the temporal variation of convection on time scales of 1–10 Ma. Recently, it has been demonstrated that transient uplift events punctuated the otherwise uniform thermal subsidence of sedimentary basins which fringe the Icelandic plume. In the Faroe–Shetland basin, three-dimensional seismic reflection surveys calibrated by well logs have been used to reconstruct a ∼55 million year old transient event. The minimum amount of uplift is 490 m, which grew and decayed within 2 Ma. This event has also been mapped 400 km further east in the North Sea basin, where peak uplift with an amplitude of 300 m occurred 0.3–1.6 Ma later. Neither observation can be explained by glacio-eustatic sea-level changes or by crustal shortening. We describe a simple fluid dynamical model which accounts for these transient and diachronous observations. In this model, we assume that the Icelandic plume was already in existence and that it had an axisymmetric geometry in which hot (e.g. 1400 °C) asthenospheric material flows away from a central conduit within a horizontal layer. A transient temperature anomaly introduced at the plume centre flows outward as an expanding annulus. Its geometry is calculated using radial flow between two parallel plates with a Poiseuille cross-stream velocity profile. The expanding annulus of hot asthenosphere generates transient isostatic uplift at the Earth's surface. Stratigraphic observations from both basins can be accounted for using a plume flux of 1.3×10^8 km^3 Ma^{-1} for a layer thickness of 100 km. Plume flux is broadly consistent with that required to account for Neogene (0–20 Ma) V-shaped ridges south of Iceland, although our transient temperature anomalies are larger. We suspect that the stratigraphic expression of transient convective behaviour is common and that a careful examination of appropriate records could yield important insights.
© 2007 Elsevier B.V. All rights reserved.

1. Introduction

Although there is general agreement that plate motions are maintained by thermal convection in the Earth's mantle, we still know rather little about the spatial and temporal details of the convective flow. Thus any observations that can be used to constrain the nature of this circulation are of particular interest. This paper is concerned with the detailed Paleogene stratigraphy of the northwest continental margin of Europe, which we believe yields a record of one aspect of the time dependence of convective flow.

Numerical and laboratory experiments of high Rayleigh number convection demonstrate that the resulting flow is strongly time-dependent (White and McKenzie, 1995; Larsen and Yuen, 1997; Schubert et al., 2001). When the Rayleigh number is increased beyond ∼10^5, steady three-dimensional circulation begins to oscillate periodically. It does so in one of two ways: either by varying velocity whilst preserving the planform of steady flow; or by generating an oscillating planform. When the Rayleigh number is increased further, these oscillations become

* Corresponding author. Bullard Laboratories, Department of Earth Sciences, Madingley Rise, Madingley, Road, Cambridge CB3 0EZ, UK. Tel.: +44 1223 337176; fax: +44 1223 360779.
E-mail addresses: rudge@esc.cam.ac.uk (J.F. Rudge), shaw@esc.cam.ac.uk (M.E. Shaw Champion), nwhite@esc.cam.ac.uk (N. White), mckenzie@esc.cam.ac.uk (D. McKenzie), lovell@esc.cam.ac.uk (B. Lovell).

larger and more irregular. If the planform remains unchanged, such oscillations can give rise to large intermittent blobs of hot and cold fluid which are transported around the convection cell. Here we refer to such blobs as pulses. If planform oscillations grow, they often cause the planform itself to alter (e.g. pairs of hot or cold plumes can join together). We use the term plume in its fluid dynamical sense, to refer to any region of fluid that is rising or sinking because of its buoyancy, without any implications concerning the composition of material involved or the vertical extent of motion. Plume fusion proceeds until the boundary layers become unstable at which point new hot and cold plumes form by the growth of instabilities. If the Rayleigh number is increased still further to $\sim 10^{10}$, convective circulation ceases to have any organized planform and heat is now transported through the isothermal interior by rising and sinking blobs generated from boundary layer instabilities.

The Rayleigh number of the Earth's mantle is 10^6–10^8, depending on whether convection occurs within one or two layers. We thus expect the convective flow to be time-dependent although it should still possess a planform. Hot blobs generated by instabilities of the lower boundary layer are widely believed to be responsible for building large igneous provinces (e.g. Early Cenozoic volcanism of the North Atlantic Ocean White and McKenzie, 1995). In the Pacific Ocean, the plume beneath Hawaii has generated a long volcanic ridge as the Pacific Plate moves over it. Relative motion between this plume and the overlying plate changed rapidly ~ 42 Ma ago. Tarduno et al. (2003) used paleomagnetic observations to show that this change was caused by a change in the velocity of the plume of ~ 30 mm a^{-1} in a reference frame fixed to the North Pole. Other plumes in the North Atlantic and Indian Oceans do not show the same change in velocity which demonstrates that the convective planform is time-dependent. Furthermore, variable bathymetry of the Hawaiian Ridge requires the plume temperature itself to vary on time scales of a few million years (Vogt, 1979; Davies, 1992; O'Connor et al., 2002). Even shorter period variations may also occur but cannot easily be resolved.

Time-dependent mantle convection should produce corresponding changes in elevation of the Earth's surface. Large igneous provinces are often accompanied by regional uplift caused by impingement of a hot blob on the base of the lithosphere (White and McKenzie, 1989). At smaller scales, temperature fluctuations within the plume should also cause spatial and temporal changes in surficial elevation. Unlike melt generation, which is only affected by the vertical component of velocity, uplift will also occur when hot blobs travel horizontally. Uplift and consequent denudation will be most easily detected on continental shelves where thermally subsiding sedimentary basins with low elastic thicknesses exist. High sediment supply usually maintains the fringes of these gently subsiding basins close to sea level for long periods of time and so their stratigraphic records can act as sensitive indicators of transient vertical displacements of $\sim 10^2$ m.

These general arguments imply that sedimentary basins distributed along the continental margins of the North Atlantic Ocean could record the arrival of pulses of hot asthenospheric material spreading away from the Icelandic plume. A phase of uplift, with an amplitude greater than that expected from glacio-eustatic sea-level variations, followed by rapid subsidence is evidence of transient vertical motion caused by passage of a hot pulse beneath the continental lithosphere.

In this paper, we first discuss stratigraphic evidence that such a pulse travelled outwards from the Icelandic plume during Eocene times. Then we outline a simple fluid dynamical model which accounts for these observations. Similar transient uplift events occur on both sides of the North Atlantic Ocean throughout Cenozoic and Mesozoic times. They may also be caused by transient convective phenomena. However, the amplitudes of these events are uncertain and it cannot yet be demonstrated that any of them are diachronous.

2. Stratigraphic record of vertical motions

Under certain circumstances, three-dimensional (3D) seismic reflection surveys acquired and processed by the hydrocarbon industry and calibrated by well-log information can be used to reconstruct minor transient vertical displacements which have occurred within the post-rift phase of sedimentary basins. It is more difficult to reconstruct these motions using two-dimensional seismic reflection lines or well-log data alone. In the Faroe–Shetland and North Sea basins, the availability of 3D seismic data, combined with detailed biostratigraphy based on a large number of wells, has yielded detailed histories of vertical displacements, particularly from Paleogene strata which were deposited close to ancient sea level. In this section, we review the evidence for these displacements and the methodology behind their reconstruction.

2.1. The Faroe–Shetland basin

Smallwood and Gill (2002) described and interpreted 3D seismic data from the southern part of the Faroe–Shetland basin (the Judd area, Fig. 1). In particular, they documented a Late Paleocene–Early Eocene history of change in water depth and elevation. Shaw Champion et al. (in press) extended this analysis to a wider area. They also quantified the history of vertical motions relative to sea level by correcting for the effects of later crustal shortening, differential sediment compaction and isostatic loading.

Fig. 2 shows the stratigraphy of the area during Late Paleocene to Early Eocene times. An obvious feature is an unconformity which separates the Lamba and Flett/Balder Formations. Fig. 3a shows the results of mapping this unconformity surface on 3D seismic data. There is clear evidence of incision into underlying marine sediments and development of a dendritic drainage network which feeds a substantial meandering channel (Fig. 3). The minimum amount of uplift responsible for generation of this incised surface can be estimated by constructing a surficial envelope once the effects of subsequent compaction and of isostatic loading are removed. Shaw Champion et al. (in press) have shown that the original tectonic uplift was at least 490 m. An incised surface cut into relatively unconsolidated sediments has limited preservation potential unless it is rapidly buried. Well data show that this surface was quickly buried.

Constraints on the timing of vertical motions were obtained by dating sedimentary rocks deposited on top of the incised surface. The oldest sedimentary rocks, which cover the incised surface, are terrestrial sandstones interbedded with coal and lignite layers which belong to the Lower Flett Formation (i.e. T40 sequence of Lamers and Carmichael, 1999). This formation is correlated to the Forties Formation of the North Sea (Mudge and Bujak, 2001). By tying key biomarkers to the chronostratigraphy of Luterbacher et al. (2004), this sequence spans 56.1–54.8 Ma. This range yields an uncertainty in timing of peak uplift when the incised surface first began to subside and infill. When the Upper Flett Formation started to be deposited at 54.8 Ma, 215 m of the original uplift remained. Complete burial of the incised surface is demonstrably diachronous over the region, burial occurring earlier in the west. This observation implies that a component of westward tilting occurred during subsidence. Once the Balder Formation was deposited at 54.2 Ma, uplift had largely disappeared. These chronostratigraphic constraints show that the phase of transient uplift lasted 0.5–1.9 Ma. Note that the Lower Flett formation started to be deposited before 54.8 Ma so a reasonable upper bound for

peak uplift is 55.0 Ma. Thus, uplift of >490 m peaked between 56.1 and 55.0 Ma and had largely decayed within 1.9 Ma. The reconstructed history of vertical motions is shown in Fig. 4a.

2.2. The Northern North Sea

Underhill (2001) has described a record of transient vertical motion within the Late Paleocene–Early Eocene stratigraphy of the Bressay area, which is located at the eastern edge of the Shetland platform of the North Sea (Fig. 1). The Bressay area has a very similar geological record of vertical motions to that observed in the Faroe–Shetland basin. Using 3D seismic reflection data calibrated by well-log information, he mapped an erosional surface which is incised into deltaic sedimentary rocks of the Dornoch Formation (Figs. 2 and 3). This incised surface was initially infilled with a terrestrial sandstone unit (the Bressay Sandstone) which is synchronous with the upper part of the Dornoch Formation. It was later draped by the Balder Formation which is demonstrably marine (Underhill, 2001). Thus uplift died away within 0.6 Ma. The phase of uplift which
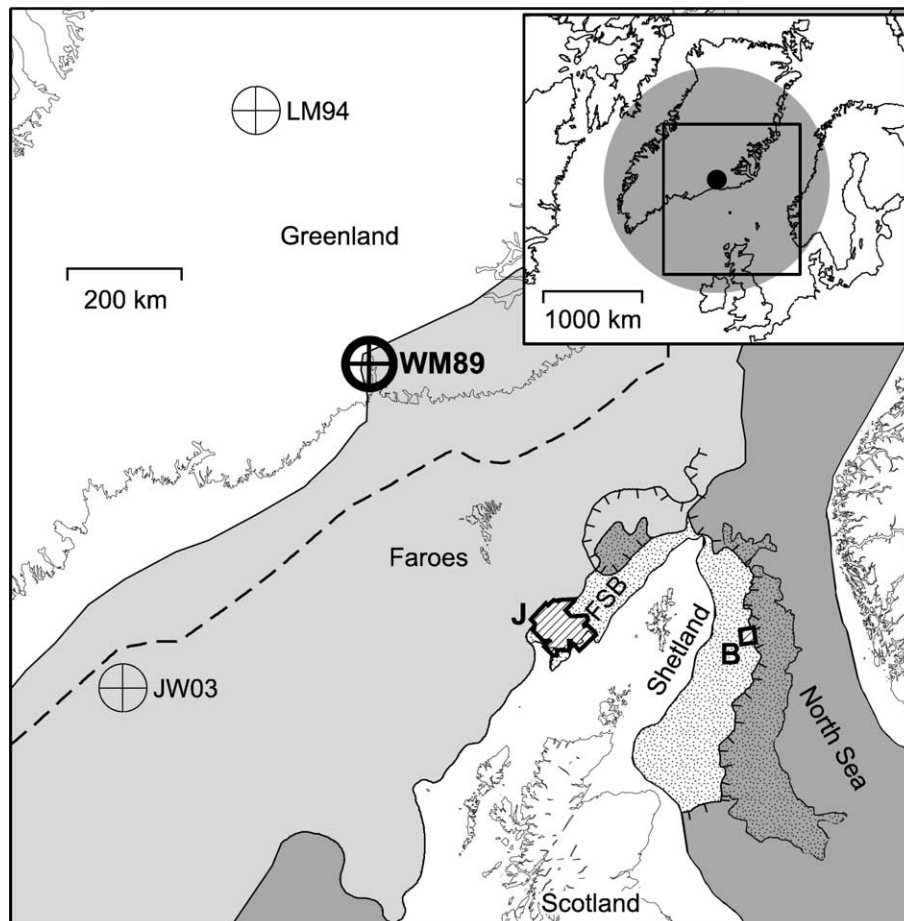

Fig. 1. Highly simplified paleogeographical reconstruction of North Atlantic Ocean during Early Eocene times (55 Ma). Crossed circles = possible locations of Icelandic plume centre at this time: WM89 = (White and McKenzie, 1989), LM94 = (Lawver and Müller, 1994), JW03 = (Jones and White, 2003); hatched areas marked J and B = Judd and Bressay areas where observations of vertical motions have been documented; light grey areas = Late Paleocene–Early Eocene volcanic rocks; plain white areas = putative landmass; white stippled regions = deltaic tops where ticked line indicates topset–foreset break; dark grey areas = zones of marine deposition; stippled areas = sand-dominated fans sourced from Scotland–Shetland landmass. Inset is idealized reconstruction of North Atlantic Ocean showing extent of influence of Early Eocene Icelandic plume after White and McKenzie, 1989 and location of main figure.
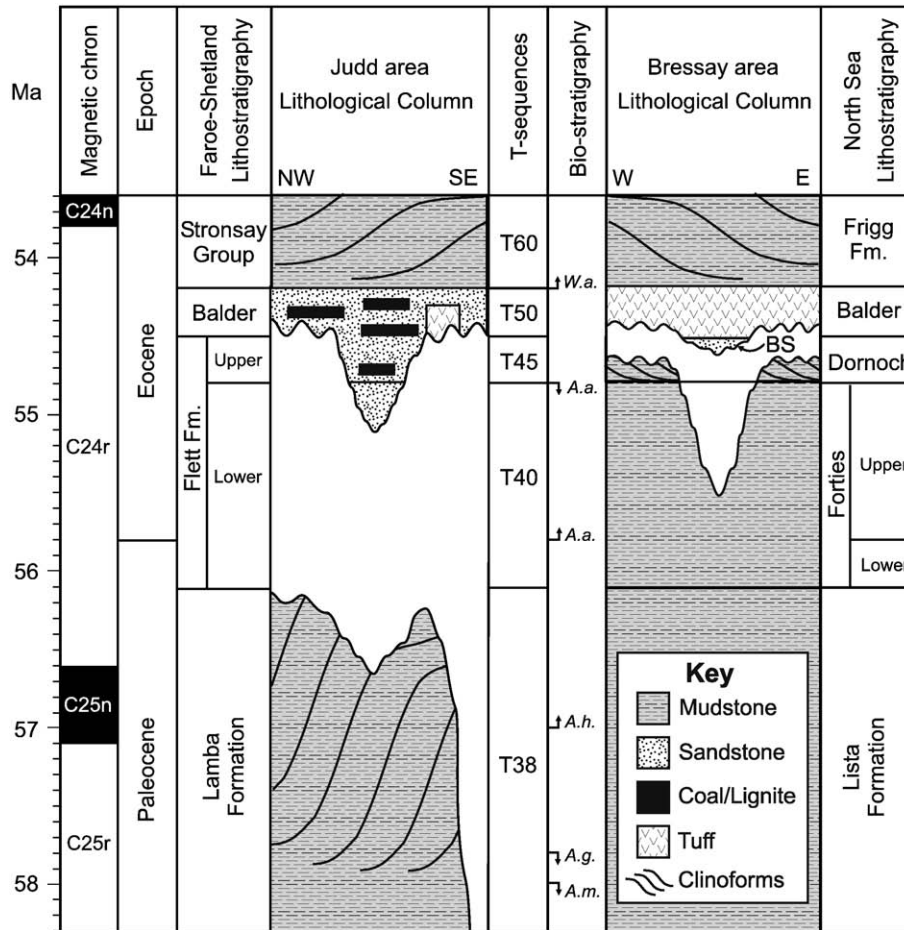
Fig. 2. Stratigraphic columns of Judd and Bressay areas located in Faroe–Shetland and northern North Sea basins, respectively. See Shaw Champion et al. (in press), Underhill (2001) for further details. Lithostratigraphic and biostratigraphic correlations follow (Mudge and Jones, 2004). Absolute dating of biostratigraphy follows Luterbacher et al., 2004. BS = Bressay Sandstone. First and last appearances of key biostratigraphic indicators are shown where *W.a.* = *Wetzeliella astra*, *A.a.* = *Apectodinium augustum*, *A.h.* = *Apectodinium homomorphum*, *A.g.* = *Areoligera gippingensis*, and *A.m.* = *Alisocysta margarita*.

produced this incised surface must have occurred during deposition of the Dornoch Formation (i.e. 54.7–54.5 Ma) which is slightly younger than the phase of uplift which occurred in the Faroe–Shetland basin.

Underhill (2001) showed that the minimum amount of uplift in the Bressay area was 250 m. This value is based on the maximal present-day thickness of the Bressay sandstone infill of the incised surface and was not corrected for post-depositional compaction of the sandstone unit or for isostatic loading. Using Shaw Champion et al.'s method (in press), the decompacted (i.e. depositional) thickness of this unit is 320 m. In this case, the component of uplift generated by an isostatic response to erosional unloading is ∼10% of the measured relief on the incised surface. Hence the minimum amount of tectonic uplift experienced in the Bressay area is ∼300 m. Our reconstructed history of vertical motions at Bressay is shown in Fig. 4b.

The Bressay area is situated some 300 km east of the Judd area and evidently suffered a similarly rapid phase of uplift and subsidence. However, the magnitude of uplift was clearly smaller and it occurred as 0.3–1.6 Ma later. In both cases, transient uplift is manifest by strikingly similar stratigraphic

responses: fluvial systems incised into deltaic sedimentary rocks to produce an erosional surface which was initially in-filled by terrestrial sedimentary rocks and later overlain by marine sedimentary rocks of the Balder Formation. Underhill (2001) has noted that incision in the Bressay area is not uniform along the length of the Dornoch deltaic system. Thus transient uplift and/or its stratigraphic expression is heterogeneous. Our mapping of 3D seismic reflection surveys north of the Bressay area shows that only minor incision occurred east of the major normal faults which bound the edge of the East Shetland Platform. We suggest that the stratigraphic expression of transient uplift is probably affected by a combination of paleo-geography and crustal structure. For the purposes of this paper, transient uplift measurements at Bressay are regarded as representative of the western edge of the northern North Sea.

3. The cause of transient uplift events

We have described transient uplift events from the northwest continental shelf of Europe which have a number of important features which help to prescribe their origin. First, it is generally accepted that these events are regional but not global in
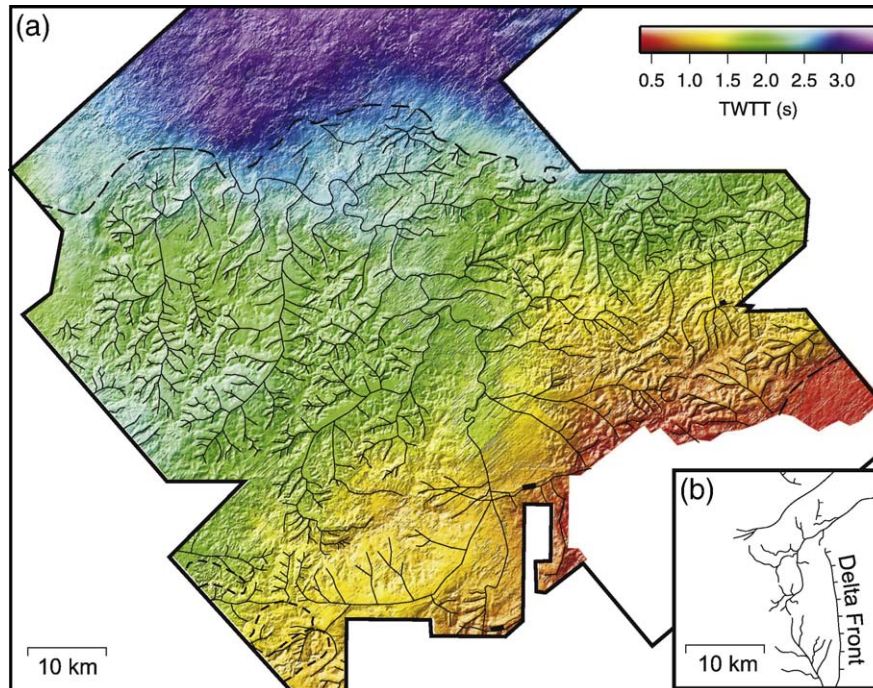
Fig. 3. Buried Paleogene surfaces mapped from 3D seismic reflection surveys. (a) Incised unconformity surface beneath Judd area of Faroe–Shetland basin (after Shaw Champion et al., in press); (b) drainage pattern on incised surface beneath Bressay area of northern North Sea basin at the same scale (after Underhill, 2001). See Fig. 1 for locations.

their extent. Secondly, we are confident that the Judd–Bressay transient event was diachronous. Thirdly, uplift is of the order of 0.5 km and decays as rapidly as it appears. Clearly, these particular events cannot be accounted for either by glacio-eustatic variations in sea level or by phases of crustal shortening. The similarity of both reconstructed uplift histories as well as associated erosional and sedimentary responses supports the notion that these events have a common causal mechanism.

Dynamical topography is easily generated by emplacing anomalously hot, and thus buoyant, asthenospheric material beneath continental lithosphere. Since the velocity of a convective flow can exceed plate velocities, rapid and short-duration uplift events can be produced by the convective emplacement and removal of anomalously hot asthenosphere. We propose a mechanism whereby an anomalously hot portion of plume material is advected beneath the Faroe–Shetland and North Sea basins thus accounting for the rapid and diachronous uplift events described above. This explanation is predicated upon the existence of lateral flow of asthenosphere from northwest to southeast away from the centre of the Icelandic convective plume and beneath the continental margin.

In a mantle plume, buoyant material rises vertically through a thin (∼100 km wide) conduit and spreads laterally as it impinges on the base of the lithosphere, generating a plume head. We assume a simple axisymmetric model of the plume head with a plume centre located northwest of the Faroe Islands. The exact location of the Early Paleogene plume centre is much debated. Based on the distribution of Early Paleogene igneous activity, White and McKenzie (1989) suggested that the area affected by the plume could be roughly delineated by a circle ∼1000 km in diameter, centred on East Greenland (Fig. 1). A

reconstruction of the Icelandic plume track within an assumed hotspot frame of reference locates the plume centre beneath central Greenland at ∼55 Ma (Lawver and Müller, 1994). More recently, Jones and White (2003) determined the position of the centre of the plume swell from estimates of dynamic support of the coastline of the British Isles. Their best-fitting model is centred close to the line of continental break-up, southwest of the Faroe Islands. All three locations are possible end-members for the position of the plume centre used in our model (Fig. 1). Regardless of the exact location of the plume centre, a plume head would have underlain much of the North Atlantic region and its centre was situated west or northwest of the continental shelf under consideration.

If a pulse of anomalously hot plume material is supplied from the plume stem, it will travel radially outwards when it reaches the base of the lithosphere. The simplest model of propagation of such a pulse is one-dimensional radial advection. From conservation of mass, the radial velocity $u_r \propto 1/r$. The position of a pulse is thus $r^2 = k (t - t_0)$, where k is a parameter measured in units of diffusivity (km^2 Ma^{-1}) which characterizes the speed of the pulse, and t_0 is the time when the pulse leaves the origin. Since we have information about uplift at two different positions, it is possible to estimate the parameters k and t_0. Suppose that peak uplift occurs at radius r_1 at time t_1, and subsequently at radius r_2 at time t_2. Then k can be calculated from

$$k = \frac{r_2^2 - r_1^2}{t_2 - t_1}. \qquad (1)$$

There are uncertainties associated with both the timing of each peak uplift and the position of the centre of the plume.
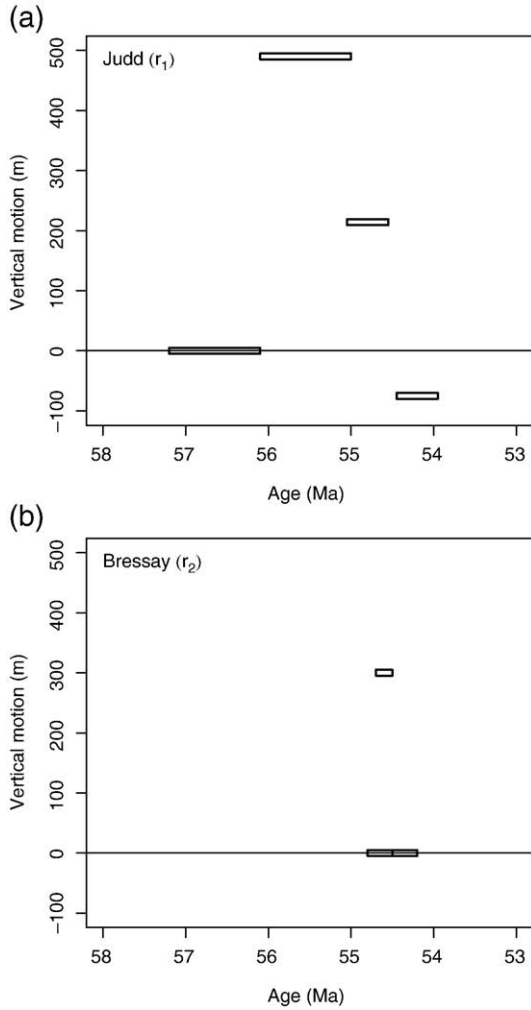
Fig. 4. Estimates of transient uplift and subsidence from (a) Judd area of Faroe–Shetland basin and (b) Bressay area of northern North Sea basin. Rectangles indicate dating constraints. Note there are two adjacent rectangles on the 0 m line of (b).

Table 1 shows three estimates of distances from the plume centre with corresponding values of $r_2^2 - r_1^2$, which vary by a factor of 2. Peak uplift is thought to have occurred between 56.1 and 55.0 Ma in the Judd area and between 54.7 and 54.5 Ma in the Bressay area (Fig. 4). These timings lead to a range of estimates for $t_2 - t_1$ of between 0.3 and 1.6 Ma, varying by a factor of 5. Hence estimates for k range over an order of magnitude, from $k = 2.1 \times 10^5$ to 2.1×10^6 km^2 Ma^{-1}. The corresponding range of estimates for t_0 lies between 55.3 and 60.2 Ma and depends strongly on the location of the plume centre.

Table 1
Radial distances from three proposed plume centres out to areas which record uplift: Judd (r_1) and Bressay (r_2)

Plume centre	r_1 (km)	r_2 (km)	$r_2^2 - r_1^2$ (km^2)	r_2/r_1
WM89 (White and McKenzie, 1989)	580	820	336,000	1.41
LM94 (Lawver and Müller, 1994)	1070	1260	442,700	1.18
JW03 (Jones and White, 2003)	770	1100	617,100	1.43

There is more information contained in the reconstructed vertical motions (Fig. 4) than just timing of peak uplift: we also know about the amount of uplift that occurred and we have constraints on the decay of uplift. This information may be used to provide better estimates of the timing of the pulse and its duration. To exploit these data, we have developed a simple kinematic model of advection and diffusion of heat within a plume head. The mathematical details of this model are described in the Appendices and a summary of notation is given in Table F.1.

4. A simple model of a plume head

The viscosity of the mantle is governed by temperature, pressure, the presence of partial melt, and degree of dehydration. Models of the temperature and pressure structure of the mantle, of experimental studies of rock rheology, and of seismic observations have led numerous authors to argue for the presence of a low viscosity zone in the upper asthenospheric mantle [e.g. Richter and McKenzie, 1978; Buck and Parmentier, 1986; Robinson et al., 1987; Robinson and Parsons, 1988; Ceuleneer et al., 1988; Rabinowicz et al., 1990; Hirth and Kohlstedt, 1996]. This low viscosity zone is thought to be at most 200 km thick with a typical viscosity 10–100 times lower than that determined from studies of post-glacial rebound. The lateral flow of a plume head is assumed to be concentrated in this low viscosity zone.

Here we consider a highly idealized kinematic model of an established plume head which is shown in Fig. 5. This model consists of an axisymmetric radial flow between two parallel plates with a Poiseuille (parabolic) cross-stream velocity profile. Flow is prescribed by a volume flux, Q, and by a layer thickness, $2h$. The precise geometry and flow profile of a real plume will obviously be more complicated but our idealization is a useful starting point for the purposes of this paper. It is also sufficiently similar to flow profiles observed in more sophisticated numerical models [e.g. Ito, 2001].

We can study the effect of temperature perturbations on this pre-existing flow. Our kinematic model does not specify the origin of a temperature anomaly, which is supplied to the plume head up the conduit. A hotter region of material could be entrained in the plume, ultimately originating from the boundary layer which feeds the plume. Alternatively, a perturbation could originate as a result of the development of a solitary wave within the plume conduit [e.g. Scott et al., 1986; Olson and Christensen, 1986; Ito, 2001]. If temperature perturbations are sufficiently small then they will not adversely affect the underlying flow. Thus excess temperature can be treated as a passive tracer: it is simply advected by the flow and can diffuse but it has no back effect on the flow. Such temperature perturbations will cause uplift and subsidence at the surface. The amount of uplift and subsidence is linearly related to the average excess temperature across the layer. Isostatic considerations show that

$$U = \frac{2h\alpha\overline{T}}{1 - \alpha T_0}, \tag{2}$$

where U is the surface uplift, $2h$ is the layer thickness, α is the thermal expansivity, T_0 is the background temperature, and $\overline{T}$ is
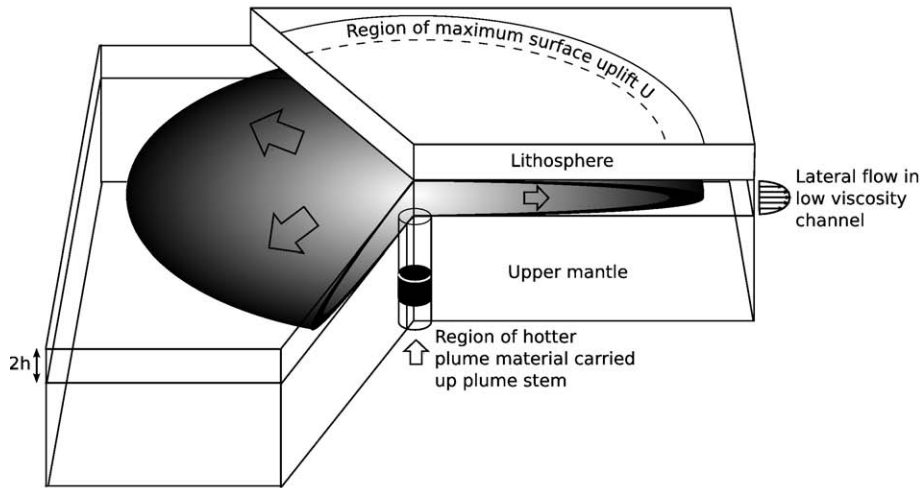
Fig. 5. Cartoon which illustrates the geometry of our simplified plume model.

the average temperature across the layer in excess of the background. If the wavelength of the anomaly is large compared to the elastic thickness of the lithosphere, flexural effects can be ignored and the assumption of Airy isostasy is valid. The elastic thickness of old oceanic lithosphere is ~30 km. Such lithosphere will only undergo uplift when the horizontal extent of a hot blob is ~300 km. In contrast, stretched and subsided continental lithosphere has an elastic thickness of ≤5 km and will be much more responsive to small changes in the thermal structure of a convective planform.

Eq. (2) shows the trade-off between the thickness of a plume head layer and the average temperature anomaly within it, which together act to produce a given amount of surface uplift. Due to this trade-off, it is helpful to place independent limits on the likely magnitude of the temperature anomaly. Neogene temperature pulses responsible for generating the V-shaped ridges north and south of Iceland are thought to have been up to ~35 °C greater than background temperature (Smallwood and White, 1998). A V-shaped ridge south of the Azores plume probably formed by a significantly hotter anomaly (~130 °C) (Escartin et al., 2001). Here we use a likely bound for the average temperature anomaly of 150 °C. Assuming that the background temperature of the plume was 1400–1500 °C, some 100–200 °C above normal, the upper bound for the temperature of a pulse is 1550–1650 °C. Such a temperature anomaly is unlikely to generate significant amounts of melt beneath unstretched lithosphere (White and McKenzie, 1995), consistent with the absence of melting at this time away from the incipient North Atlantic rift. Fig. 6 shows that a plume head layer thickness of 100–200 km with such a temperature anomaly can easily produce the observed 500 m uplift.

There are three significant time scales in our model: the time scales for radial advection, for radial diffusion, and for cross-layer diffusion. The balance between radial advection and diffusion is characterized by the Péclet number, $Pe = q/\kappa$, where q is the average area flux ($q = Q/2h$, a typical value is $q = 1.3 \times 10^6$ km^2 Ma^{-1}) and κ is the thermal diffusivity (typical value $\kappa = 31$ km^2 Ma^{-1}). Thus the Péclet number is large, $Pe \sim 4 \times 10^4$, and radial advection dominates over radial dif-

fusion. The importance of cross-layer diffusion depends on the layer half-thickness, h, which we assume to be ~50 km. Thus the thermal time constant for the layer, $h^2/\pi^2\kappa$, is ~8 Ma. Since transient uplift and subsidence took place over ~2 Ma, only a small amount of cross-layer diffusion occurs during this time.

4.1. The purely advective case

The preceding time-scale considerations motivate a model that neglects diffusion completely and considers only pure advection. Such a model is described in detail in Appendix B. A Gaussian pulse of temperature is imposed at the origin with peak temperature occurring at time t_0. The standard deviation has a time δ and the amplitude is determined by parameter S. The peak of this pulse travels at the maximum cross-stream speed and so k is related to the average area flux q by $k = 3q/2\pi$.
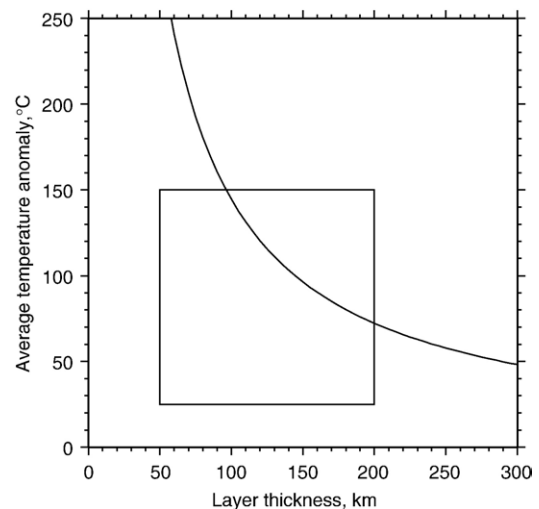

Fig. 6. Trade-off between plume head layer thickness, $2h$, and average excess temperature across this layer, T. All combinations of $2h$ and T on the curve produce a surficial uplift of 500 m (Eq. (2)). Our calculations assume thermal expansivity of $\alpha = 3.3 \times 10^{-5}$ °C^{-1} and background layer temperature of $T_0 = 1400$ °C (note that the model is insensitive to T_0). Box denotes geologically reasonable ranges for layer thickness and excess temperature.

Advection of the pulse away from the origin can be used to calculate uplift curves at any radial distance from the plume centre. Four unknown parameters specify the model: k, t_0, δ, and S. A summary of the model is shown in Fig. 7.

The stratigraphic constraints from the two locations described in Section 2 are used to specify a model that produces a good fit to the reconstructed vertical motions. The fit to the observations is shown in Fig. 8a and b. The plume centre location of White and McKenzie (1989) pins distances to positions of observed uplift. The amplitude of the initial pulse was chosen to match peak uplift in the Judd area. k and t_0 are chosen indirectly by setting times t_1 and t_2 of maximum uplift at the two locations. t_1 has been chosen as 55.15 Ma, close to the end of the interval dictated by stratigraphic uncertainties (56.10–55.00 Ma). This choice of t_1 facilitates fitting of the later data point in the Judd area. t_2 is more tightly constrained by the stratigraphy of the Bressay area and it has been chosen as 54.60 Ma within the middle of the range of uncertainty (54.70–54.50 Ma). The standard deviation, δ, has been chosen as 0.04 Ma to give an appropriate match to the duration of the pulse observed at the two locations, which is again better constrained in the Bressay area. As a result, $k = 6.11 \times 10^5$ km^2 Ma^{-1} and $t_0 = 55.74$ Ma.

An important prediction of our model is that peak uplift should be smaller at greater distances from the plume centre. This decay is clearly observed: the Judd area has a peak uplift of 490 m and the Bressay area has a peak uplift of 300 m. The model also predicts that the ratio of peak uplifts is approximately r_2/r_1. This ratio is listed in Table 1 for different locations of the plume centre and should be compared with the ratio of uplift magnitudes in the two areas (i.e. 490/300 = 1.63). For all choices of plume centre, r_2/r_1 is slightly higher than the uplift ratio, hence the slight overshoot for the uplift curve in Fig. 8b. The model also predicts that the duration of uplift should be longer the further away from the plume centre. Unfortunately, the onset and duration of transient uplift must be estimated from stratigraphic excision and as yet it is impossible to resolve these details. We tentatively suggest that both areas must have been exposed for similarly short durations since drainage patterns with strikingly similar geomorphological expression have been incised into very similar substrates. Finally, it must be stressed that our model assumes a uniform thickness plume head layer. If the layer thickness was allowed to vary laterally, the width and hence duration of a pulse would be strongly affected.

Our predicted uplift phases do not decay as rapidly as the stratigraphic constraints suggest as is evident from the presence
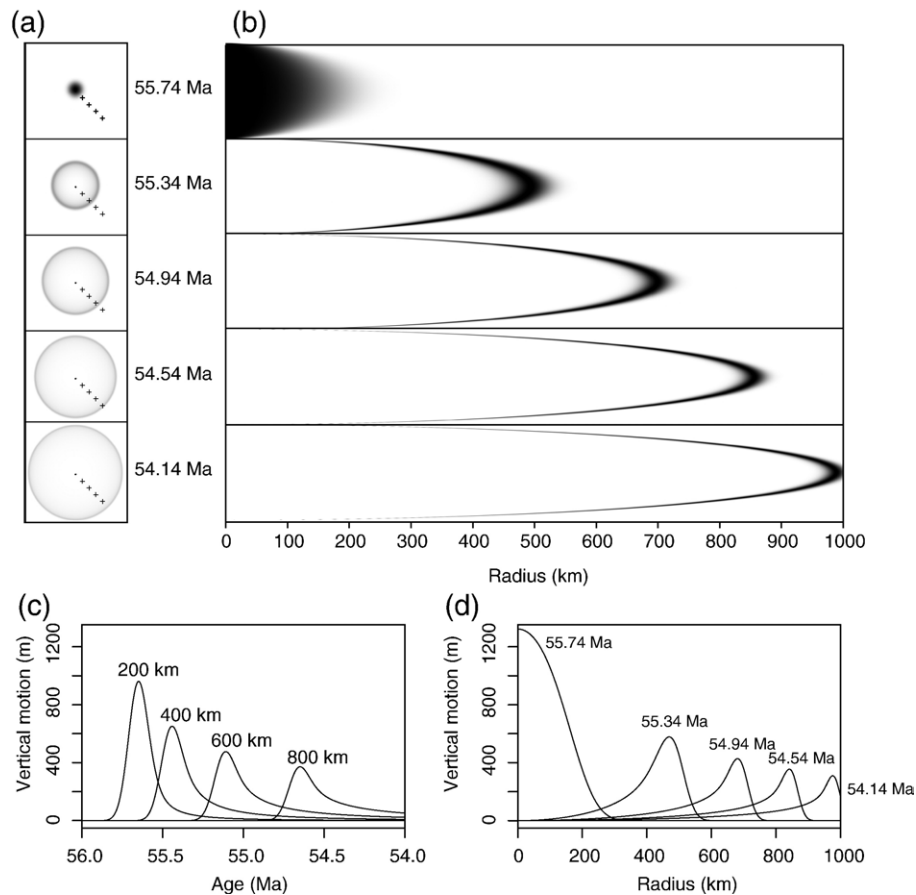

Fig. 7. Calculations for purely advective model. Values of parameters are same as those given in Fig. 8a and b. (a) Plan view at five different times where greyscale intensity shows cross-sectionally averaged temperature. Crosses mark four observation stations at 200, 400, 600 and 800 km distance from plume centre. (b) Cross section through layer where greyscale shows excess temperature. (c) Averaged temperature converted to surficial uplift as a function of time for each of the four observation stations. (d) Surficial uplift plotted as a function of radius at the five times shown in (a) and (b).
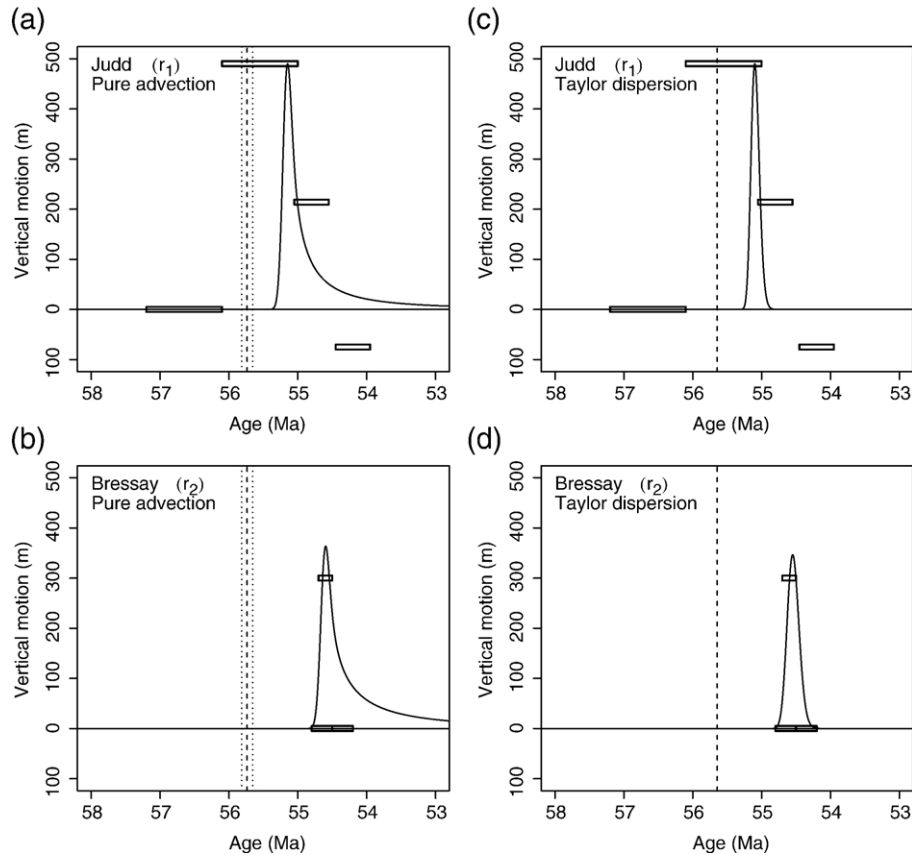
Fig. 8. Estimates of uplift and subsidence which have been fitted with two different theoretical models. (a), (b) Purely advective model results for Judd (r_1) and for Bressay (r_2). Fits were chosen so that peak uplift at $r_1 = 580$ km occurs at $t_1 = 55.15$ Ma while peak uplift at $r_2 = 820$ km occurs at $t_2 = 54.60$ Ma. This difference sets $k = 6.1 \times 10^5$ km^2 Ma^{-1}. Initial input is a Gaussian pulse of temperature at the origin, centred about $t_0 = 55.74$ Ma (dashed vertical line). Standard deviation is $\delta = 0.04$ Ma ($t_0 \pm 2\delta$ interval given by dotted vertical lines). Average area flux $q = 2\pi k/3 = 1.28 \times 10^6$ km^2 Ma^{-1} which yields a volume flux $Q = 2hq = 1.28 \times 10^8$ km^3 Ma^{-1} for a layer half-height $h = 50$ km. (c), (d) Taylor dispersion model results for Judd (r_1) and for Bressay (r_2). Fits were chosen so that peak uplift at $r_1 = 580$ km occurs at $t_1 = 55.1$ Ma while peak uplift at $r_2 = 820$ km occurs at $t_2 = 54.55$ Ma. This difference sets $k = 6.1 \times 105$ km^2 Ma^{-1} and $t_0 = 55.65$ Ma (dashed vertical line). The fixed Gaussian width is chosen with standard deviation $\sigma_r = 40$ km. The average area flux $q = \pi k = 1.92 \times 10^6$ km^2 Ma^{-1}, leading to a plume flux $Q = 2hq = 1.92 \times 10^8$ km^3 Ma^{-1} for a layer half-height $h = 50$ km.

of the long 'tails'. We suspect that the reason for this discrepancy arises from the complex way in which a transient uplift is translated into a stratigraphic response whilst the specific paleogeographical framework evolves. Nevertheless, the fact that the principal features of the uplift data (i.e. amplitude, duration, timing, rate) can be replicated with a simple model is very encouraging. It should be noted that the model does not include a uniform background rate of thermal subsidence that would shift the model curve downwards with increasing time, producing a better fit. We must also add that although time-scale arguments show that a purely advective solution is appropriate, some diffusion will act to smear out the sharper gradients. Thus thin regions seen in the cross-section of Fig. 7 will smooth out and reduce the extent of the long tails in Fig. 8a and b. Tails are potentially consistent with one stratigraphic observation: westward tilting of the Judd area during the decay of uplift.

4.2. Taylor dispersion

Simple time-scale arguments suggest that cross-layer diffusion is unimportant. Nevertheless, it is interesting to examine what happens when the time scale for cross-layer diffusion is comparable to the advective time. Such a regime is discussed in detail in Appendix C, and the analysis is essentially standard Taylor dispersion theory (Taylor, 1953). Taylor dispersion occurs when a combination of cross-stream velocity gradients and cross-stream diffusion causes along-stream spreading, which is often characterized by an enhanced effective diffusivity along-stream. In the well-studied problem of solute released in a pipe with Poiseuille flow, the concentration profile eventually becomes uniform in the cross-stream direction and travels in the along-stream direction with a Gaussian shape at the mean velocity where the width spreads diffusively as $\sim t^{1/2}$. A similar phenomena occurs in this model but with one important difference: because of its axisymmetric geometry (Fig. 5), the pulse does not spread as it would in the standard Taylor dispersion problem. Instead, it travels with a Gaussian shape which has an approximately constant along-stream width. For an initially short-duration pulse, this width can be determined from the Péclet number and layer thickness (see Eq. (C.8)). Since the pulse travels at the mean velocity rather than at the maximum velocity, the relationship between pulse speed and average area flux is given by $k = q/\pi$.

This model also has four free parameters: k, t_0, S, and σ_r, the standard deviation of the constant along-stream width. Fig. 8c and d shows a fit to the data using the solution from Taylor dispersion theory. The same fitting procedure is followed as before with the choice of t_1 and t_2 determining k and t_0. Pulse speed is again set at $k = 6.11 \times 10^5$ km^2 Ma^{-1}, with a starting time of $t_0 = 55.65$ Ma. Peak uplifts are related through r_1/r_2 and uplift duration scales linearly with radius. The fixed radial width is chosen as $\sigma_r = 40$ km in order to match uplift durations. For an initially short-duration pulse, the radial width should be related to the Péclet number and layer thickness. However, such a σ_r implies an unrealistically thin layer ($h \approx 3$ km). Thus although the fit is somewhat improved for a Taylor dispersion model especially since tails are absent, we maintain that a purely advective parameter regime is more geologically realistic.

5. Discussion

An important underlying assumption of our model is that the plume head was present beneath the region by earliest Eocene times. We can then assume a simple flow geometry within the plume head into which a temperature anomaly is introduced. Previous authors have modelled the impact of a plume head on the base of the lithosphere as a spreading gravity current (Bercovici and Lin, 1996; Vasilyev et al., 2001). We show in Appendix E that a gravity current model cannot explain the transient vertical motions described here. Instead, we suggest that plume impact occurred during Paleocene times, conceivably as a gravity current. Our best-fitting model exploits a purely advective regime which replicates key features of the observed vertical motions. Such a model makes several predictions about plume behaviour which could have wider implications.

First of all, it is instructive to compare our predictions with the velocities, sizes and shapes of temperature pulses inferred to have produced the Neogene V-shaped ridges, which straddle the mid-oceanic ridges north and south of Iceland. Vogt (1971) originally estimated a pulse velocity $u_{pulse} = 200$ km Ma^{-1} at a distance of 600 km from the plume centre (an order of magnitude greater than the plate spreading velocity of ~ 20 km Ma^{-1}). If these pulses are generated by temperature anomalies which travel radially then this pulse velocity implies that $k = 2ru_{pulse} = 2.4 \times 10^5$ km^2 Ma^{-1}. Revised pulse velocity estimates vary from 250 km Ma^{-1} at distances < 700 km to 100 km Ma^{-1} at distances > 700 km (Jones et al., 2002). This range yields a k of 1.4–3.5×10^5 km^2 Ma^{-1}. In Fig. 8, we used a pulse area flux of $k = 6.1 \times 10^5$ km^2 Ma^{-1} which is about twice that needed to explain the V-shaped ridges. The youngest V-shaped ridges have widths of ~ 300 km (Jones et al., 2002) which agrees well with our predictions.

It is encouraging that estimates of k determined using two very different approaches are similar to within one order of magnitude. If these estimates are accurate, we conclude that plume flux decreased by about a factor of two over the last 50 Ma. It is probably reasonable to expect higher fluxes during the early stages of a plume's history. Initiation of mantle plumes is frequently manifested by emplacement of large igneous pro-

vinces (LIPs) whose rapid eruption rates require elevated plume fluxes. In order to compare pulse area flux k, which is determined from uplift histories and V-shaped ridge geometries, with a plume's volume flux, Q, which can be estimated by independent means, we use the relationship $Q = 4\pi hk/3$. If the plume head layer thickness, $2h$, is ~ 100 km then $Q \approx 1.3 \times 10^8$ km^3 Ma^{-1}. The volume flux required to account for the Neogene V-shaped ridges is approximately half this value since it scales linearly with k ($Q \approx 0.3$–0.7×10^8 km^3 Ma^{-1}). The volume, geochemistry and geochronology of flood basalts from the North Atlantic Igneous Province should provide an independent estimate of the Icelandic plume's flux at its initiation. There are considerable uncertainties but we assume that 10^6–10^7 km^3 of basalt were underplated and erupted within 1–3 Ma (White and McKenzie, 1995, 1989). If the degree of melting was $\sim 10\%$, we obtain a flux of plume material through the melting region of 0.3–1×10^8 km^3 Ma^{-1}. This estimate is reasonably similar to the flux required by our model and by analysis of V-shaped ridge geometries.

Ito (2001) developed a three-dimensional numerical simulation of plume flow in which pulsed temperature anomalies induced beneath a spreading ridge generate V-shaped ridges. In his model, a pulse "attains a steady-state along-axis width", which is precisely what is found in the Taylor dispersion regime of our model. Ito's model reproduces the general morphology of Neogene V-shaped ridges but it does not match their migration velocities. His simulations have $q \approx 7 \times 10^4$ km^2 Ma^{-1}, with corresponding pulse speeds $k \approx 3.0 \times 10^4$ km^2 Ma^{-1} (based on maximum velocity, pure advection) or $k \approx 2.0 \times 10^4$ km^2 Ma^{-1} (based on mean velocity, Taylor dispersion). Thus Ito's numerical solution has advection an order of magnitude slower than that expected from observations of V-shaped ridges, and up to 30 times slower than the fits of our model. As a result of slower advection, cross-layer diffusion is more important which may explain why behaviour more akin to the Taylor dispersion solution is observed.

There is some independent evidence that the Icelandic plume exhibited short-period temporal dependency before Neogene times. Mid-Eocene oceanic crustal thickness and free-air gravity measurements northeast of the Faroe Islands are consistent with a pulse in plume temperature with a duration of ~ 2–4 Ma (Parkin et al., 2007). This observation was made ~ 300–400 km from the Early Eocene plume centre position of White and McKenzie (1989). Fig. 7c shows that at this radial distance, we predict a pulse with a duration of 0.25–0.5 Ma which is shorter than the Mid-Eocene pulse recorded by oceanic thickness variation. The duration of the pulse sampled at a fixed point depends on both its width and speed. If a Mid-Eocene pulse travelled with a velocity similar to those which produced the Neogene V-shaped ridges then it would have a width consistent with our results.

The model presented here provides a satisfactory explanation for Early Eocene transient vertical motions recorded in the Faroe–Shetland and northern North Sea basins. We have focused on these particular transient events for three reasons. First, transient events which punctuate the uniform thermal subsidence phases of sedimentary basins are easily identifiable.

Secondly, the hydrocarbon industry have generously made available 3D seismic reflection surveys calibrated by detailed biostratigraphy which allow us to quantify with some degree of confidence the amplitudes and durations of these particular events. Thirdly, the northwest continental shelf of Europe developed in close proximity to the evolving Icelandic mantle plume whose temporal and spatial evolution is known at least in outline. We are aware that similar transient uplift events as well as episodic phases of clastic deposition have been identified in the Paleogene sequences of Northwest Europe (White and Lovell, 1997; Dam et al., 1998; Maclennan and Lovell, 2002; Mudge and Jones, 2004). In the absence of reliable estimates of amplitude and duration and– crucially– a demonstration that they are diachronous, it is difficult to be certain that these events are not caused by glacio-eustatic sea-level changes. Nevertheless, transient convective behaviour is unlikely to be confined to the Icelandic plume and such behaviour should manifest itself in the global stratigraphic record, albeit under particular palaeoenvironmental conditions.

6. Conclusions

Mapping of 3D seismic reflection surveys, calibrated by biostratigraphy from well-log data, has revealed the existence of rapid, short-lived, transient uplift in both the Judd area of the Faroe–Shetland basin and in the Bressay area at the western edge of the northern North Sea. Reconstruction of the amount of incision constrains the minimum amount of uplift in each case. Stratigraphic considerations show that a phase of >490 m uplift in the Judd area preceded >300 m uplift in the Bressay area by 0.3–1.6 Ma. Both phases were short-lived but it is difficult to give precise estimates. As far as we can tell, Judd uplift peaked and decayed within a maximum of 1.6 Ma whilst the Bressay event only lasted 0.3 Ma.

We have described a simple kinematic model of radial flow within an existing plume head. Flow occurs within a horizontal layer with a Poiseuille cross-stream profile. A thermal anomaly is introduced at the plume centre which is positioned close to the line of North Atlantic continental break-up (White and McKenzie, 1989). The anomaly flows outwards as an expanding annulus and generates transient uplift at the Earth's surface which fits the reconstructed vertical motions in both basins. The temperature of this anomaly (75–150 °C beneath the Judd area) trades off against the thickness of the plume head layer (100–200 km). Nevertheless, the range of values required to reproduce the observations are consistent with independent estimates. Our model is conceptually similar in some respects to models previously used to explain Neogene V-shaped ridge formation (Ito, 2001; Jones et al., 2002).

Two parameter regimes were considered. The first one assumes pure advection and ignores diffusion of heat. The second one assumes a time scale for cross-layer diffusion which is comparable to the advective time. A realistic parameter regime lies somewhere between the two extremes of pure advection and Taylor dispersion but it is probably closer to the purely advective end member. We obtain a good fit to the reconstructed vertical motions when the hot pulse has a Gaussian distribution, originating at $t_0 = 55.74$ Ma with standard deviation $\delta = 0.04$ Ma. The model is most tightly constrained by stratigraphic data from the Bressay area, which place limits on the duration and timing of peak uplift. We can best fit data from the Judd area when peak uplift is placed at the younger bound of stratigraphic uncertainty. Although we obtain improved fits by using the Taylor dispersion model, we maintain that this parameter regime is not geologically realistic.

The application of this simple model makes several predictions, the most important of which concerns the plume flux required to reproduce a pulse velocity which matches the stratigraphic constraints. A volume flux estimate of 1.3×10^8 km^3 Ma^{-1} is broadly consistent with independent estimates calculated from Neogene V-shaped ridge geometries and from arguments based on flood basalt eruption rates. We suggest that Early Eocene plume flux was approximately double the present-day value.

Acknowledgements

Appendices

A. Model details

Consider radial outflow between two parallel plates at $z = \pm h$ (Fig. 5). The velocity field is purely radial and takes the form

$$u(r,z) = \frac{q}{2\pi r} f(z/h) \tag{A.1}$$

where the function $f(z/h)$ describes the cross-stream variation in velocity. A simple Poiseuille profile will be assumed so that

$$f(z/h) = \frac{3}{2}\left(1 - (z/h)^2\right) \tag{A.2}$$

with normalization 3/2 chosen so that the mean value across the stream is 1. If Q is the total volume flux from the source, then $q = Q/2h$ is the mean area flux. The maximum velocity across the stream is given by $u_{max}(r) = 3q/4\pi r$ and the mean velocity across the stream by $\bar{u}(r) = q/2\pi r$.

Temperature perturbations will affect this flow through changes in buoyancy (the term $\rho_0 \alpha \Delta T g$ in the momentum equation). However, we will assume such buoyancy effects are small and can be neglected. Excess temperature can then be

treated as a passive scalar: it is advected by the flow and diffuses but it has no back effect on the flow. The temperature field is thus described by an advection–diffusion equation

$$\frac{\partial T}{\partial t} + u(r,z)\frac{\partial T}{\partial r} = \kappa\frac{\partial^2 T}{\partial z^2} + \kappa\frac{1}{r}\frac{\partial}{\partial r}\left(r\frac{\partial T}{\partial r}\right) \tag{A.3}$$

with zero heat flux boundary conditions on the plates such that

$$\frac{\partial T}{\partial z} = 0 \quad \text{on } z = \pm h \tag{A.4}$$

and suitable initial conditions and boundary conditions at $r=0$ and as $r \to \infty$.

The main quantity of interest is the cross-sectional average of temperature, $\bar{T}(r, t)$, which is defined by

$$\bar{T}(r,t) = \frac{1}{2h}\int_{-h}^{h} T(r,z,t)\,dz, \tag{A.5}$$

rather than the temperature profile $T(r, z, t)$ per se. The amount of uplift and subsidence at the surface is linearly related to $\bar{T}(r, t)$ through Eq. (2).

A key non-dimensional parameter characterizing this model is the Péclet number $Pe=q/\kappa$ which determines the relative importance of radial advection and diffusion. Here it is assumed that Pe is large so that radial advection dominates. As a result, only at very short and at very long times is the radial diffusion term in Eq. (A.3) important, and we neglect it in the following (see Section D of the appendix for further discussion). Substitution of the velocity field (Eq. (A.1)) into Eq. (A.3) then yields

$$\frac{\partial T}{\partial t} + \frac{q}{2\pi r}f(z/h)\frac{\partial T}{\partial r} = \kappa\frac{\partial^2 T}{\partial z^2}. \tag{A.6}$$

This equation can be simplified by introducing a new area co-ordinate $a=\pi r^2$ so that

$$\frac{\partial T}{\partial t} + qf(z/h)\frac{\partial T}{\partial a} = \kappa\frac{\partial^2 T}{\partial z^2}. \tag{A.7}$$

This modification yields another advection–diffusion equation which is easier to analyse because the advection no longer depends on the streamwise co-ordinate. In fact, Eq. (A.7) describes the well-studied problem of a tracer within a unidirectional two-dimensional flow between two parallel plates. It is convenient to non-dimensionalise Eq. (A.7) using

$$t = \frac{h^2}{\kappa}t', \quad a = \frac{qh^2}{\kappa}a', \quad z = hz'. \tag{A.8}$$

Eq. (A.7) then becomes

$$\frac{\partial T}{\partial t'} + f(z')\frac{\partial T}{\partial a'} = \frac{\partial^2 T}{\partial z'^2}. \tag{A.9}$$

In general, this equation must be solved numerically. However, for small and large values of the non-dimensional time, t', simple analytical solutions exist which are discussed in the next two appendices.

B. Pure advection

Suppose that the initial temperature profile is uniform in the z-direction and that the boundary conditions are also uniform in z. At early times $t' \ll 1$ (i.e. $t \ll h^2/\kappa$), the system is dominated by advection and the cross-stream diffusion term can be neglected so that

$$\frac{\partial T}{\partial t'} + f(z')\frac{\partial T}{\partial a'} = 0. \tag{B.1}$$

The most general solution of (B.1) is given by

$$T(a',z',t') = g(a' - f(z)t', z'), \tag{B.2}$$

where $g(\eta', z')$ is a function which will be specified by the initial and boundary conditions. In dimensional form, this solution can be written as

$$T(r,z,t) = h(\pi r^2 - f(z/h)qt, z) \tag{B.3}$$

where $h(\eta, z)$ is similarly specified by the initial and boundary conditions.

B.1. Boxcar pulse

As a simple example, consider the problem of a boxcar pulse of temperature at the origin with a duration of time τ. This problem is described by the initial condition $T \equiv 0$ for $t < 0$, and boundary condition

$$T(0,z,t) = \frac{S}{q\tau}\begin{cases} 1 & 0 < t < \tau, \\ 0 & \text{otherwise}, \end{cases} \tag{B.4}$$

where the normalization $S/q\tau$ has been chosen so that for $t > \tau$

$$\int_0^\infty \bar{T}(r,t)2\pi r\,dr = S. \tag{B.5}$$

It also follows that for any $r > 0$

$$\int_{-\infty}^\infty \bar{T}(r,t)q\,dt = S. \tag{B.6}$$

The solution of the pure advection problem is simply

$$T(r,z,t) = \frac{S}{q\tau}\begin{cases} 1 & q(t-\tau)f(z/h) < \pi r^2 < qtf(z/h), \\ 0 & \text{otherwise}. \end{cases} \tag{B.7}$$

Hence for $0 < t < \tau$,

$$\bar{T}(r,t) = \frac{S}{q\tau}\begin{cases} \sqrt{1-\dfrac{r^2}{kt}} & 0 < r^2 < kt, \\ 0 & r^2 > kt \end{cases} \tag{B.8}$$

and for $t > \tau$

$$\bar{T}(r,t) = \frac{S}{q\tau}\begin{cases} \sqrt{1-\dfrac{r^2}{kt}} - \sqrt{1-\dfrac{r^2}{k(t-\tau)}} & 0 < r^2 < k(t-\tau), \\ \sqrt{1-\dfrac{r^2}{kt}} & k(t-\tau) < r^2 < kt, \\ 0 & r^2 > kt \end{cases} \tag{B.9}$$

where $k = 3q/2\pi$. Note that the peak of the pulse is at the origin for $t < \tau$ and at $r^2 = k(t - \tau)$ for $t > \tau$. The peak thus travels at the maximum velocity $u_{\max}(r) = k/2r = 3q/4\pi r$. The amplitude of the peak is $S/q\tau$ for $t < \tau$ and $(S/q\tau)(\tau/t)^{1/2}$ for $t > \tau$.

B.2. Very short pulse

In the case of a very short-duration pulse, $\tau \ll t$, the averaged temperature can be approximated by

$$\overline{T}(r,t) = \begin{cases} \dfrac{S\pi r^2}{3q^2 t^2}\left(1 - \dfrac{r^2}{kt}\right)^{-1/2} & 0 < r^2 < kt, \\ 0 & r^2 > kt \end{cases} \tag{B.10}$$

except in a small region near the pulse peak where there is a singularity. This solution has a self-similar structure

$$\overline{T}(r,t) = \frac{S}{2qt} b(\zeta) = \frac{3S}{4\pi r^2} \zeta b(\zeta) \tag{B.11}$$

where $\zeta = r^2/kt$ and

$$b(\varsigma) = \begin{cases} \zeta(1 - \zeta)^{-1/2} & 0 < \zeta < 1, \\ 0 & \zeta > 1. \end{cases} \tag{B.12}$$

The peak of the pulse is at $r^2 = kt$, so again the pulse moves at the maximum velocity $u_{\max}(r)$. The pulse spreads out over time, increasing in length at the same rate as the pulse moves. The overall amplitude decays as t^{-1}.

B.3. Gaussian pulse

An unfortunate feature of the boxcar pulse of subsection B.1 is the sharp edge when it is switched on and then off, resulting in a discontinuous temperature gradient. A smooth temperature profile can be produced by considering a Gaussian pulse in temperature at the origin with a boundary condition of the form

$$T(0,z,t) = \frac{S}{(2\pi)^{1/2} q\delta} e^{-t^2/2\delta^2} \tag{B.13}$$

where δ is the standard deviation of the imposed Gaussian pulse, which leads to the general solution

$$T(r,z,t) = \frac{S}{(2\pi)^{1/2} q\delta} e^{-\left(\pi r^2/qf(z/h) - t\right)^2/2\delta^2}. \tag{B14}$$

There is no simple analytic expression for $\overline{T}(r, t)$ but it is straightforward to calculate $\overline{T}(r, t)$ numerically. The behaviour of this solution is expected to be similar to that of the boxcar solution with a peak moving out the maximum velocity $u_{\max}(r)$ and peak amplitude decreasing as $t^{-1/2}$.

C. Taylor dispersion

For long times $t' \gtrsim 1$ (i.e. $t \gtrsim h^2/\kappa$), there is a well-known reduction of (A.9) due to Taylor (1953). In this regime, the temperature is uniform in the z' direction (so $T = \overline{T}$), and it is described by a one-dimensional advection–diffusion equation in the a' direction

$$\frac{\partial T}{\partial t'} + \frac{\partial T}{\partial a'} = D'_{\text{eff}} \frac{\partial^2 T}{\partial a'^2}, \tag{C.1}$$

where $D'_{\text{eff}} = 2/105$ is the effective diffusivity (Wooding, 1960). For the initial release of a pulse $T(a', 0) = \delta(a')$ there is the simple Gaussian solution

$$T(a',t') = \frac{1}{\left(4\pi D'_{\text{eff}} t'\right)^{1/2}} e^{-(a'-t')^2/4D'_{\text{eff}} t'}. \tag{C.2}$$

In dimensional variables, the governing equation is

$$\frac{\partial T}{\partial t} + q\frac{\partial T}{\partial a} = D_{\text{eff}} \frac{\partial^2 T}{\partial a^2} \tag{C.3}$$

where

$$D_{\text{eff}} = \frac{2}{105} \frac{q^2 h^2}{\kappa} \tag{C.4}$$

or in terms of r

$$\frac{\partial T}{\partial t} + \frac{q}{2\pi r}\frac{\partial T}{\partial r} = \frac{D_{\text{eff}}}{4\pi^2 r}\frac{\partial}{\partial r}\left(\frac{1}{r}\frac{\partial T}{\partial r}\right). \tag{C.5}$$

It is important to notice that while the right-hand side of Eq. (C.3) is a diffusive term with respect to the a variable, the right-hand side of Eq. (C.5) is not a diffusive term with respect to the r variable. The pulse release solution is

$$T(r,t) = \frac{S}{\left(4\pi D_{\text{eff}} t\right)^{1/2}} e^{-\left(\pi r^2 - qt\right)^2/4D_{\text{eff}} t} \tag{C.6}$$

which can be further simplified by expanding about the mean position of the pulse $\mu_r = (qt/\pi)^{1/2}$ to obtain

$$T(r,t) = \frac{S}{(2\pi)^{3/2} \mu_r \sigma_r} e^{-(r-\mu_r)^2/2\sigma_r^2}, \tag{C.7}$$

where

$$\sigma_r = \left(\frac{D_{\text{eff}}}{2\pi q}\right)^{1/2} = \left(\frac{Pe}{105\pi}\right)^{1/2} h. \tag{C.8}$$

The approximation represented by Eq. (C.7) is formally valid for $|r - \mu_r| \ll \mu_r$, which in turn is valid if $t \gg h^2/105\kappa$. Since $t \gtrsim h^2/\kappa$ in order for the solution (C.6) to be valid then (C.7) should always be a good approximation within this regime.

There are three key results. First, the pulse is positioned around $\mu_r = (qt/\pi)^{1/2}$ and so the pulse moves with the mean velocity $\bar{u}(r) = q/2\pi r$. Secondly, the pulse does not spread in this regime but instead has an approximately fixed half-width σ_r. Thirdly, the pulse amplitude decays as $t^{-1/2}$.

Stone and Brenner (1999) have also studied this Taylor dispersion problem. They claim that the solution (C.6)

demonstrates a sub-diffusive spreading in r with spreading about the mean scaling as $t^{1/4}$. This claim is mistaken. When profiles of (C.6) are plotted and by inspection of the approximation used in (C.7), it is clear that no such spreading occurs. It should also be noted that a similar approximation to (C.7) can be made in terms of t so that

$$T(r,t) = \frac{S}{(2\pi)^{1/2} q \sigma_t} e^{-(t-\mu_t)^2/2\sigma_t^2} \qquad (C.9)$$

where $\mu_t = \pi r^2/q$ and $\sigma_t = 2\pi r \sigma_r/q$. This approximation is valid for $|t - \mu_t| \ll \mu_t$.

D. Radial diffusion

Thus far, the radial diffusion term

$$\kappa \frac{1}{r} \frac{\partial}{\partial r} \left(r \frac{\partial T}{\partial r} \right) \qquad (D.1)$$

has been neglected. In terms of the non-dimensional Eq. (A.9), the missing term on the right-hand side is

$$\frac{4\pi}{Pe} \frac{\partial}{\partial a'} \left(a' \frac{\partial T}{\partial a'} \right) = \frac{4\pi}{Pe} \left(\frac{\partial T}{\partial a'} + a' \frac{\partial^2 T}{\partial a'^2} \right). \qquad (D.2)$$

Since we are assuming that the Péclet number is large, this term can be neglected under most circumstances. The main effect of including this term will be to smooth radial temperature profiles over a length scale $(2\kappa t)^{1/2}$. Radial diffusion will be important at very early times, in smoothing any initially steep gradients in temperature, and at very late times $t' \sim D'_{\text{eff}} Pe/4\pi = Pe/210\pi$, when (D.2) will become comparable to the diffusive term on the right-hand side of (C.1). For these very late times $(t' \gg Pe/210\pi)$ the temperature field takes the form

$$T(r,t) = \frac{S}{(2\pi)^{3/2} \mu_r (2\kappa t)^{1/2}} e^{-(r-\mu_r)^2/4\kappa t}. \qquad (D.3)$$

This profile spreads as $(2\pi t)^{1/2}$ and its amplitude decays as t^{-1}.

E. Gravity current models

Mantle plume heads are often modelled as gravity currents (Bercovici and Lin, 1996; Vasilyev et al., 2001). In this section, we show that existing gravity current models cannot explain the transient uplift phenomena described in this paper. Consider the classical problem of a blob of isoviscous fluid spreading axisymmetrically under gravity on top of a rigid plate (Huppert, 1982). The thickness, $H(r,t)$, of the fluid layer has a similarity solution of the form

$$H(r,t) = Bt^{-1/4} f \left(r/At^{1/8} \right) \qquad (E.1)$$

where A and B are dimensional constants, and $f(\eta) = (1-\eta^2)^{1/3}$. This spreading blob can be regarded as a model of a starting plume head where a region of hotter mantle material spreads beneath rigid lithosphere. For an isothermal blob, the thickness $H(r,t)$ will be linearly related to surficial uplift. From Eq. (E.1), it can be seen that the blob spreads very slowly with $r \sim t^{1/8}$ (compared with $r \sim t^{1/2}$ of our model). Thus while there will be rapid uplift at a given position as the nose of the blob travels beneath, the subsidence which follows will be very gradual, its amplitude decaying as $t^{-1/4}$.

A faster spreading gravity current can be generated if there is a continual injection of new material. With a constant rate of injection, the layer thickness $H(r,t)$ is

$$H(r,t) = Bf \left(r/At^{1/2} \right), \qquad (E.2)$$

where A and B are now different dimensional constants and $f(\eta) = (1-\eta^2)^{1/3}$. This current spreads in the same way as our model $(r \sim t^{1/2})$. However, there is no subsidence at all.

These examples are simple cases but more sophisticated schemes with different boundary conditions and more realistic rheologies such as Bercovici and Lin (1996), Vasilyev et al. (2001) are equally unlikely to produce rapid subsidence. For example, if the material cools as it spreads out, it becomes more viscous and spreading slows down (Bercovici and Lin, 1996). To generate rapid subsidence, we have based our model on temperature perturbations within a pre-existing flow. Of course, this background flow could conceivably be supplied by a gravity current model but for simplicity we have chosen to use an idealized flow.

Table F.1
Notation

Symbol	Quantity		Units
a	Area co-ordinate	πr^2	m^2
D_{eff}	Effective area diffusivity	$2q^2 h^2/105\kappa$	m^4 s^{-1}
h	Layer half-height		m
k	Pulse area flux (pure advection or Taylor)	$3q/2\pi$ or q/π	m^2 s^{-1}
Pe	Péclet number	q/κ	–
Q	Total volume flux		m^3 s^{-1}
q	Average area flux	$Q/2h$	m^2 s^{-1}
r	Radial co-ordinate		m
S	Total area integrated $\overline{T}$	(B.5)	°C m^2
$T(r,z,t)$	Temperature		°C
$\overline{T}(r,t)$	Cross-sectionally averaged temperature		°C
t	Time		s
$u(r,z)$	Radial velocity		m s^{-1}
$\overline{u}(r)$	Cross-sectionally averaged velocity	$q/2\pi r$	m s^{-1}
$u_{\text{max}}(r)$	Maximum cross-stream velocity	$3q/4\pi r$	m s^{-1}
z	Vertical co-ordinate		m
α	Thermal expansivity		°C^{-1}
δ	Std. dev. in time of Gaussian pulse at origin		s
κ	Thermal diffusivity		m^2 s^{-1}
μ_r	Mean position of Taylor dispersion pulse	$(qt/\pi)^{1/2}$	m
μ_t	Mean timing of Taylor dispersion pulse	$\pi r^2/q$	s
σ_r	Std. dev. of position in Taylor dispersion pulse	$(D_{\text{eff}}/2\pi q)^{1/2}$	m
σ_t	Std. dev. of timing in Taylor dispersion pulse	$2\pi r \sigma_r/q$	s
τ	Total duration of boxcar pulse at origin		s

References

Bercovici, D., Lin, J., 1996. A gravity current model of cooling mantle plume heads with temperature-dependent buoyancy and viscosity. J. Geophys. Res. 101, 3291–3309. doi:10.1029/95JB03538.

Buck, W.R., Parmentier, E.M., 1986. Convection beneath young oceanic lithosphere: implications for thermal structure and gravity. J. Geophys. Res. 91, 1961–1974.

Ceuleneer, G., Rabinowicz, M., Monnereau, M., Cazenave, A., Rosemberg, C., 1988. Viscosity and thickness of the sub-lithospheric low-viscosity zone: constraints from geoid and depth over oceanic swells. Earth Planet. Sci. Lett. 89, 84–102. doi:10.1016/0012-821X(88)90034-9.

Dam, G., Larsen, M., Sønderholm, M., 1998. Sedimentary response to mantle plumes: implications from Paleocene onshore successions, West and East Greenland. Geology 26, 207–210. doi:10.1130/0091-7613(1998)026<0207:SRTMPI>2.3.CO;2.

Davies, G.F., 1992. Temporal variation of the Hawaiian plume flux. Earth Planet. Sci. Lett. 113, 277–286. doi:10.1016/0012-821X(92)90225-K.

Escartin, J., Cannat, M., Pouliquen, G., Rabain, A., Lin, J., 2001. Crustal thickness of V-shaped ridges south of the Azores: interaction of the Mid-Atlantic Ridge (36°–39°N) and the Azores hot spot. J. Geophys. Res. 106, 21719–21735. doi:10.1029/2001JB000224.

Hirth, G., Kohlstedt, D.L., 1996. Water in the oceanic upper mantle: implications for rheology, melt extraction and the evolution of the lithosphere. Earth Planet. Sci. Lett. 144, 93–108. doi:10.1016/0012-821X(96)00154-9.

Huppert, H.E., 1982. The propagation of two-dimensional and axisymmetric viscous gravity currents over a rigid horizontal surface. J. Fluid Mech. 121, 43–58. doi:10.1017/S0022112082001797.

Ito, G., 2001. Reykjanes "V"-shaped ridges originating from a pulsing and dehydrating mantle plume. Nature 411, 681–684. doi:10.1038/35079561.

Jones, S.M., White, N., 2003. Shape and size of the starting Iceland plume swell. Earth Planet. Sci. Lett. 216, 271–282. doi:10.1016/S0012-821X(03)00507-7.

Jones, S.M., White, N., Maclennan, J., 2002. V-shaped ridges around Iceland: implications for spatial and temporal patterns of mantle convection. Geochem. Geophys. Geosyst. 3, 1059. doi:10.1029/2002GC000361.

Lamers, E., Carmichael, S.M.M., 1999. The Paleocene deepwater sandstone play West of Shetland. In: Fleet, A.J., Boldy, S.A.R. (Eds.), Petroleum Geology of Northwest Europe: Proceedings of the 5th Conference. Geol. Soc. Lond. pp.645–659.

Larsen, T.B., Yuen, D.A., 1997. Ultrafast upwelling bursting through the upper mantle. Earth Planet. Sci. Lett. 146, 393–399. doi:10.1016/S0012-821X(96)00247-6.

Lawver, L.A., Müller, R.D., 1994. Iceland hotspot track. Geology 22, 311–314. doi:10.1130/0091-7613(1994)022<0311:IHT>2.3.CO;2.

Luterbacher, H.P., Ali, J.R., Brinkhuis, H., Gradstein, F.M., Hooker, J.J., Monechi, S., Ogg, J.G., Powell, J., Rohl, U., Sanfilippo, A., Schmitz, B., 2004. The Paleogene Period. In: Gradstein, F.M., Ogg, J.G., Smith, A.G. (Eds.), A Geologic Time Scale 2004. Cambridge University Press, pp. 384–408. doi:10.2277/0521786738.

Maclennan, J., Lovell, B., 2002. Control of regional sea-level by surface uplift and subsidence caused by magmatic underplating of Earth's crust. Geology 30, 675–678. doi:10.1130/0091-7613(2002)030<0675:CORSLB>2.O.CO;2.

Mudge, D.C., Bujak, J.P., 2001. Biostratigraphic evidence for evolving palaeoenvironments in the Lower Paleogene of the Faeroe–Shetland Basin. Mar. Pet. Geol. 18, 577–590. doi:10.1016/S0264-8172(00)00074-X.

Mudge, D.C., Jones, S.M., 2004. Palaeocene uplift and subsidence events in the Scotland–Shetland and North Sea region and their relationship to the Iceland Plume. J. Geol. Soc. (Lond.) 161, 381–386. doi:10.1144/0016-764903-038.

Olson, P., Christensen, U., 1986. Solitary wave propagation in a fluid conduit within a viscous matrix. J. Geophys. Res. 91, 6367–6374.

O'Connor, J.M., Stoffers, P., Wijbrans, J.R., 2002. Pulsing of a focused mantle plume: evidence from the distribution of foundation chain hotspot volcanism. Geophys. Res. Lett. 29, 64–64. doi:10.1029/2002GL01481.

Parkin, C.J., Lunnon, Z.C., White, R.S., Christie, P.A., 2007. Integrated Seismic Imaging & Modelling of Margins Project (iSIMM) Team, imaging the pulsing Iceland mantle plume through the Eocene. Geology 35, 93–96. doi:10.1130/G23273A.1.

Rabinowicz, M., Ceuleneer, G., Monnereau, M., Rosemberg, C., 1990. Three-dimensional models of mantle flow across a low-viscosity zone: implications for hotspot dynamics. Earth Planet. Sci. Lett. 99, 170–184. doi:10.1016/0012-821X(90)90080-H.

Richter, F., McKenzie, D., 1978. Simple plate models of mantle convection. J. Geophys. 44, 441–471.

Robinson, E., Parsons, B., 1988. Effect of a shallow low-viscosity zone on the formation of midplate swells. J. Geophys. Res. 93, 3144–3156. doi:10.1029/88JB01305.

Robinson, E.M., Daly, S.F., Parsons, B., 1987. The effect of a shallow low viscosity zone on the apparent compensation of mid-plate swells. Earth Planet. Sci. Lett. 82, 335–348. doi:10.1016/0012-821X(87)90207-X.

Schubert, G., Turcotte, D.L., Olson, P., 2001. Mantle convection in the Earth and planets. Cambridge University Press. doi:10.2277/0521798361.

Scott, D.R., Stevenson, D.J., Whitehead, J.A., 1986. Observations of solitary waves in a viscously deformable pipe. Nature 319, 759–761. doi:10.1038/319759a0.

Shaw Champion, M.E., White, N., Jones, S.M., Lovell, B., Quantifying transient mantle convective uplift: An example from the Faroe–Shetland basin, Tectonics (in press), doi:10.1029/2007TC002106.

Smallwood, J.R., Gill, C.E., 2002. The rise and fall of the Faroe–Shetland Basin: evidence from seismic mapping of the Balder Formation. J. Geol. Soc. (Lond.) 159, 627–630. doi:10.1144/0016-764902-064.

Smallwood, J.R., White, R.S., 1998. Crustal accretion at the Reykjanes Ridge, 61°–62°N. J. Geophys. Res. 103, 5185–5202. doi:10.1029/97JB03387.

Stone, H.A., Brenner, H., 1999. Dispersion in flows with streamwise variations of mean velocity: radial flow. Ind. Eng. Chem. Res. 38, 851–854. doi:10.1021/ie980355f.

Tarduno, J.A., Duncan, R.A., Scholl, D.W., Cottrell, R.D., Steinberger, B., Thordarson, T., Kerr, B.C., Neal, C.R., Frey, F.A., Torii, M., Carvallo, C., 2003. The Emperor Seamounts: southward motion of the Hawaiian hotspot plume in Earth's mantle. Science 301, 1064–1069. doi:10.1126/science.1086442.

Taylor, G.I., 1953. Dispersion of soluble matter in solvent flowing slowly through a tube. Proc. R. Soc. A 219, 186–203.

Underhill, J.R., 2001. Controls on the genesis and prospectivity of Paleogene palaeogeomorphic traps, East Shetland Platform, UK North Sea. Mar. Pet. Geol. 18, 259–281. doi:10.1016/S0264-8172(00)00067-2.

Vasilyev, O.V., Ten, A.A., Yuen, D.A., 2001. Temperature-dependent viscous gravity currents with shear heating. Phys. Fluids 13, 3664–3674. doi:10.1063/1.1416501.

Vogt, P.R., 1971. Asthenosphere motion recorded by the ocean floor south of Iceland. Earth Planet. Sci. Lett. 13, 153–160. doi:10.1016/0012-821X(71)90118-X.

Vogt, P.R., 1979. Global magmatic episodes: new evidence and implications for the steady-state mid-oceanic ridge. Geology 7, 93–98. doi:10.1130/0091-7613(1979)7<93:GMENEA>2.O.CO;2.

Wessel, P., Smith, W.H.F., 1995. New version of the generic mapping tools released. Eos 76, 329–329. doi:10.1029/95E000198.

White, N., Lovell, B., 1997. Measuring the pulse of a plume with the sedimentary record. Nature 387, 888–891.

White, R., McKenzie, D., 1989. Magmatism at rift zones: the generation of volcanic continental margins and flood basalts. J. Geophys. Res. 94, 7685–7729. doi:10.1029/88JB03912.

White, R.S., McKenzie, D., 1995. Mantle plumes and flood basalts. J. Geophys. Res. 100, 17543–17586. doi:10.1029/95JB01585.

Wooding, R.A., 1960. Instability of a viscous liquid of variable density in a vertical Hele-Shaw cell. J. Fluid Mech. 7, 501–515. doi:10.1017/S0022112060000256.